CrystEngComm

Accepted Manuscript

ROYAL SOCIETY OF CHEMISTRY

www.rsc.org/crystengcomm

In the present work, the g-C_3N_4/nanocage ZnS composite photocatalyst was fabricated and the photocatalytic activity was enhanced under visible-light irradiation.

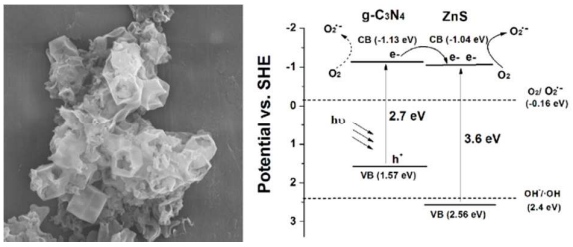

CrystEngComm RSCPublishing

ARTICLE

Fabrication of novel g-C_3N_4/nanocage ZnS composites with enhanced photocatalytic activities under visible light irradiation

Jing Wang,[*a] Peng Guo,[b] Qiangsheng Guo,[c] Pär G. Jönsson,[a] and Zhe Zhao [*a,c]

Cite this: DOI: 10.1039/x0xx00000x

Received 00th January 2012,
Accepted 00th January 2012

DOI: 10.1039/x0xx00000x

www.rsc.org/

In order to develop efficient visible light-driven photocatalysts for environmental applications, novel g-C_3N_4/nanocage ZnS composites have successfully been fabricated via an anion exchange route using ZIF-8 as a self-sacrificing template. The as-prepared g-C_3N_4/ZnS composites were characterized by powder X-ray diffraction, scanning electron microscopy, transmission electron microscopy, UV-vis diffuse reflection spectroscopy, fourier transform infrared spectroscopy and photoluminescence. In addition, the photocatalytic oxidation of organic contaminants in aqueous solution was investigated with the g-C_3N_4/ZnS composites system under visible light irradiation by using Rhodamine B as a model compound. The results indicate that the g-C_3N_4/ZnS composite photocatalysts show a higher photocatalytic activity than single component (pure g-C_3N_4 or ZnS). More specifically, the optimum photocatalytic activity of g-C_3N_4/ZnS composite was achieved with a weight ratio of 6:1, which is as high as 37.8 and 2.8 times of the individual ZnS and g-C_3N_4 under visible light irradiation. The enhanced photocatalytic activity of g-C_3N_4/ZnS is mainly attributed to an efficient electron-hole separation at the interface of the two semiconductors, as determined by photoluminescence spectroscopy. Moreover, it is observed that $\cdot O_2^-$ is the main active species in the photocatalytic oxidation of an RhB solution using a g-C_3N_4/nanocage ZnS composite.

1. Introduction

As a potential solution to the global energy and environmental pollution, design and synthesis of artificial photocatalysts with high activities have attracted great scientific interests worldwide.[1, 2] To date, various kinds of semiconductor materials, such as metal oxides and sulfides (TiO_2, ZnO, ZnS, CdS), have been studied used as photocatalysts for photodegradation of organic pollutions.[3, 4] However, most of them display high photocatalytic activity only under the ultraviolet irradiation which account for less than 5% of the total sunlight, and thus greatly limits its practical applications. Hence, it is highly desirable to extend the active photocatalytic response to the visible light region. In recent years, polymeric graphitic carbon nitride materials (g-C_3N_4), as the most stable polymorph of carbon nitrides, has attracted increasing attention due to its outstanding catalytic and photocatalytic activity.[5-7] The g-C_3N_4 possesses a high stability with respect to thermal (up to 600°C in air) and chemical attack due to the tri-s-triazine ring structure and a high degree of condensation. Moreover, an appealing electronic structure and a medium bandgap (2.7 eV) make g-C_3N_4 a promising photocatalyst for visible light irradiation. Nevertheless, the photocatalytic efficiency of bare g-C_3N_4 is greatly limited by the high recombination rate of photogenerated electron-hole pairs.[8, 9] Therefore, several routes have been developed to improve the photocatalytic performance of g-C_3N_4, including (1) doping with metal elements; (2) doping with non-metal elements and (3) constructing g-C_3N_4-based composites. It has been proved that the composite of two semiconductors with matched band gap can promote the generation and separation of photo-induced electron-hole pairs. Thus would enhance the photocatalytic activity efficiently. Recently, Sun and co-workers fabricated g-C_3N_4-ZnO composite and an enhanced photocatalytic activity under visible light irradiation was reported.[10] The improved performance was mainly attributed to the suitably matching band levels of g-C_3N_4/ZnO composites to improve the separation efficiency of electron-hole pairs. Fu *et al*. reported that the coupling of BiOBr with g-C_3N_4 can also enhance the photocatalytic performance.[11] So far various compsites based on g-C_3N_4, Bi_2WO_6/g-C_3N_4,[12] CdS/g-C_3N_4,[13, 14] $DyVO_4$/g-C_3N_4,[15] WO_3/g-C_3N_4,[16] TaON/g-C_3N_4,[17] $SrTiO_3$/g-C_3N_4,[18] C_{60}/g-C_3N_4,[19] Ag_2O/g-C_3N_4,[20] NiS/g-C_3N_4,[21] and rGO/g-C_3N_4,[22] have been demonstrated to exhibit better photocatalytic

performance compared to pure g-C_3N_4. However, the morphology effect, which has a great impact on the properties, was not given much attention in most cases.

It is well known that the characteristic morphology of g-C_3N_4 is thin layer. In order to provide a "super highway" for photo-excited charges, efficient contacted interfaces between different components is a critical factor when we construct the semiconductor composites. If it is possible to fabricate the other component material with a flat and a relative large surface, the efficient electron transfer is easier to be realized. On the other hand, a hollow structure is desirable owing to a large surface area and a high surface permeability, which are favorable for an improved photocatalytic activity. Based on these considerations, the hollow polyhedral morphology, which was constructed by flat faces, drew our attention. To date, the template strategy is the most efficient and common method to fabricate hollow materials. Among various templates, metal-organic frameworks (MOFs) have drawn great interests due to their rich species and numerous structures for the hollow structure synthesis, especially for the non-spherical hollow ones.

ZnS is a well-known photocatalyst due to its rapid generation of electron-hole pairs but the wide bandgap (3.66eV) limited its photocatalytic performance only under UV irradiation. As a classic example of MOFs, ZIF-8 can be employed as an ideal self-sacrificing template to synthesize hollow polyhedra ZnS. This is due to its non-toxicity, thermal and chemical stability, low energy consumption and efficient zinc cations supplier. Recently, Jiang *et al* reported a fabrication of truncated rhombic dodecahedral ZIF-8 nanocrystals and hollow polyhedral ZnS nanocages using ZIF-8 as sacrificial template.[23] Inspired by the above efforts, we herein construct a novel composite photocatalyst: a g-C_3N_4/nanocage ZnS with an enhanced photocatalytic performance in the visible light region. Firstly, the g-C_3N_4 was prepared by a simple pyrolysis of urea. Next, a series of g-C_3N_4/ZnS composites with different weight ratios of ZnS nanocages were successfully fabricated. Moreover, these were characterized by various techniques such as XRD, SEM-EDS, TEM and UV-vis DRS. The obtained composites show an enhanced photocatalytic performance for degradation of RhB in an aqueous solution under a visible light irradiation in comparison to either pure g-C_3N_4 or ZnS. Based on the experimental results and a theoretical analysis, a possible mechanism that explains an enhanced photocatalytic activity of g-C_3N_4/ZnS was also proposed.

2. Experimental Section

All reagents for synthesis and analysis were commercially available and used without further treatment.

2.1 Synthesis of pure g-C_3N_4

The polymeric g-C_3N_4 was prepared by a simple pyrolysis of urea without the assistance of a template.[24, 25] In a typical synthesis, 20g of urea powder was put into an alumina crucible and dried at 80°C. Then, the urea was heated to 550°C in a Muffle Furnace at a heating rate of 10°C /min and kept for 3 h. The resultant light yellow product was collected and milled into powder for further use.

2.2 Synthesis of g-C_3N_4/ZIF-8

In a typical procedure, 0.026g g-C_3N_4 was dispersed into 40mL methanol and treated in an ultrasonic bath for 2h to obtain a uniform suspension. Subsequently, desired amounts of zinc acetate dehydrate (ZA) and 2-methylimidazole (2-MI) were added into the suspension and stirred for 5 min. Then, the suspension was aged at room temperature for 24 hours. After that, the solid was collected by centrifugation and washed with methanol and dried at 60°C for 12 h.

2.3 Synthesis of g-C_3N_4/nanocage ZnS composites

The as-prepared g-C_3N_4/ZIF-8 precursor was transferred into a round bottomed flask containing 0.1M thioacetamide, 25.0 mL ethanol and 25.0 μL water. Then the mixture was refluxed for 1 h under stirring at 85°C. Finally, the product was collected by centrifugation, washed with anhydrous ethanol and dried at 60°C for 12 h. According to this method, the g-C_3N_4/ZnS composites at different weight ratios of 60:1, 12:1, 6:1 and 1:1 were prepared and denoted as 60CNZS, 12CNZS, 6CNZS and 1CNZS, respectively. The pure ZnS was synthesized under the same conditions but without the addition of a g-C_3N_4 powder.[23] Moreover, a mechanically mixed 6CNZS sample was prepared by grinding 26 mg g-C_3N_4 and 4.3 mg ZnS as a reference in order to compare the photocatalytic activity with a 6CNZS composite.

2.4 Characterization

The crystalline phases of the samples were examined by means of X-ray Powder Diffraction (XRD, PANalytical powder X-ray diffractometer with Cu Kα1 radiation, λ=0.15406 nm). The morphologies and sizes of the products were determined by Scanning Electron Microscopy (SEM, JSM-7000F). Transmission electron microscopy (TEM) images were recorded on a JEOL-2100F with an accelerating voltage of 200 kV. Fourier transform infrared (FT-IR) spectra of the samples were recorded using a Varian 670-IR FT-IR spectrometer with an attenuated total reflectance (ATR) accessory (a Golden Gate accessory with a diamond-based ATR element). UV-vis diffuse reflectance spectra of the samples were measured in the range of 200-800 nm using Shimadzu UV-3600 and using $BaSO_4$ as the reference.

2.5 Photocatalytic activity measurement

Photocatalytic activities of the series of CNZS composites were evaluated by the degradation of RhB in an aqueous solution under a visible light irradiation. An aqueous solution of RhB (20 mL, 5mg·L^{-1}) was placed in a glass beaker, and 8.5 mg photocatalyst was then added. In order to establish the adsorption-desorption equilibrium, the suspension was stirred and ultrasonically treated in the dark for 30 min, respectively. The photocatalytic activity of the samples was tested under a

500 W Xe lamp with a UV cutoff filter (λ> 400nm). The distance between the light to the beaker is 18 cm. At the given irradiation time intervals, 0.5 mL of mixture was collect and then the slurry sample was centrifuged to separate the photocatalyst particles. The concentration of RhB was analyzed by measuring the maximum absorbance at 553 nm using a Shimadzu UV-3600 spectrophotometer.

3. Results and Discussions

As shown in Figure 1, XRD was used to characterize the crystal structures of the as-obtained 6CNZS composite, as well as for the pure g-C_3N_4 and ZnS. Two characteristic peaks of 13.7° and 27.4° in the pure g-C_3N_4 sample can be indexed as the (100) and (002) diffractions for graphitic materials, corresponding to the in-plane structural packing motif and interlayer stacking of aromatic segments, respectively.[7] An XRD analysis of pure ZnS shows its wurtzite structure (JCPDF 39-1363).[23] Moreover, the relatively broad diffraction peaks indicate the fact that ZnS nanocages are composed of small building blocks, which is consistent with a HRTEM analysis of ZnS nanocages shown in Figure. S1. As coupling these two semiconductors, the diffraction peaks of the composites are similar to the pure g-C_3N_4 pattern. However, it is worth noting that a broad band located between 47° and 58° appeared in the 6CNZS composite, which can be assigned to the (110) and (118) diffraction peaks of wurtzite ZnS. The above results indicate an effective coupling effect in the CNZS composites. In addition, the XRD patterns of the CNZS composites with different weight ratios were shown in Figure. S2.

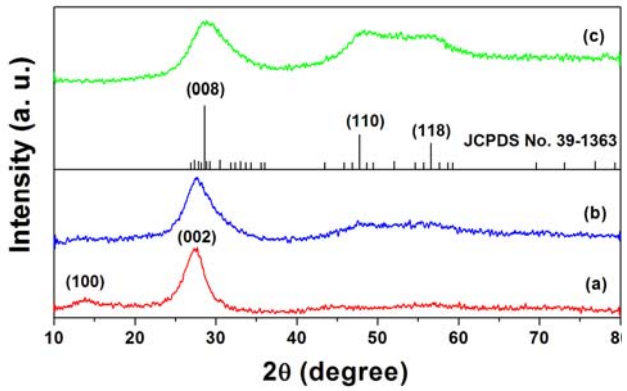

Figure 1. XRD patterns of pure g-C_3N_4, ZnS, and 6CNZS composite.

Figure 2 shows the SEM images of pure g-C_3N_4, pure ZnS nanocages, 6CNZIF-8 and 6CNZS, respectively. As shown in Figure 2a, the lamellar structure can be observed clearly in the pure g-C_3N_4 sample. Figure 2b displays the dodecahedral nanocages of pure ZnS with sizes of 0.8-1 μm, which were derived from the dodecahedral ZIF-8. The size of the nanocages can be varied by controlling the concentration and molar ratio of 2-methylimidazole and zinc acetate, as reported in previous literature.[23] After introducing the ZIF-8 to the g-C_3N_4 sample (Figure 2c), both the dodecahedral structure of ZIF-8 and the lamellar structure of g-C_3N_4 can be preserved and the average size of the ZIF-8 in 6CNZIF-8 is around 550-600 nm. The edges of the dodecahedral ZIF-8 are sharp and the facets of that are flat which can contact with g-C_3N_4 surfaces favorably. Subsequently, 6CNZS was fabricated successfully by refluxing 6CNZIF-8 with thioacetamide as sulfur source in the ethanol solvent with trace water. The hollow structure of dodecahedral ZnS can be confirmed by cracked nanocages under SEM observation. In addition, the average size of the nanocages is about 750nm, as shown in Figure 2d. Moreover, the tight contact between ZnS and g-C_3N_4 in the sample of 6CNZS was inherited from the 6CNZIF-8. Such a feature is highly desired for an efficient separation of photoinduced electron-hole pairs in composites, which will enhance the photocatalytic activity.

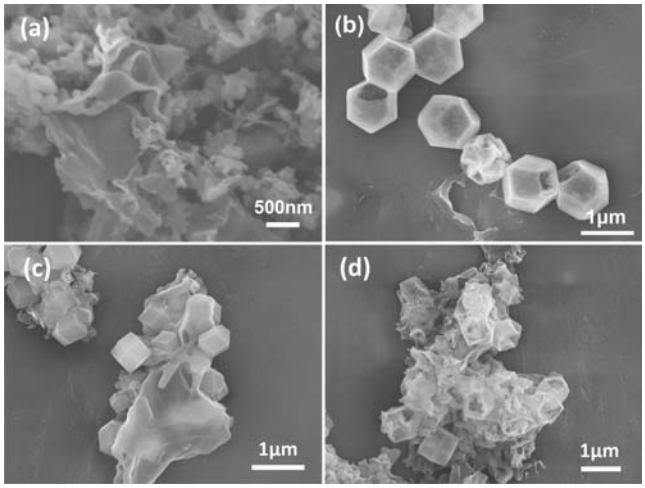

Figure 2. SEM images of (a) pure g-C_3N_4, (b) pure ZnS nanocages, (c) 6CNZIF-8, (d) 6CNZS.

In order to investigate the details of the porous structure of g-C_3N_4 and the hollow structure of ZnS nanocages, transmission electron microscopy (TEM) was employed. A TEM image of g-C_3N_4 shows typical layered platelet-like morphology with porous structure (Figure 3a), which was generated by ammonia-based gas bubbles during the pyrolysis process of urea. As shown in Figure 3b, the hollow structure of ZnS nanocages can be clearly distinguished due to the difference of electron penetrability and image contrast between the shell and inner cavity. Although some concaves are formed due to the thin shell of the nanocage, the dodecahedral morphology was maintained well. The size of the ZnS nanocage is around 650-800 nm, which is consistent with the SEM results. In order to get more detailed information about the interface between g-C_3N_4 and ZnS, the area marked by the red circle in Figure 3b is enlarged in Figure 3c by HRTEM observations. Since the in-plane diffraction (100) in a XRD pattern is weak, the corresponding lattice fringe of g-C_3N_4 is hard to find and the gray area can be assigned as the "amorphous" g-C_3N_4.[12, 15] Hence, the lattice fringes in HRTEM should be ascribed to ZnS, and the interplanar distance between the adjacent lattice fringes are 0.308 nm and 0.198 nm, which can be indexed as the (008) and (110) crystallographic plane of

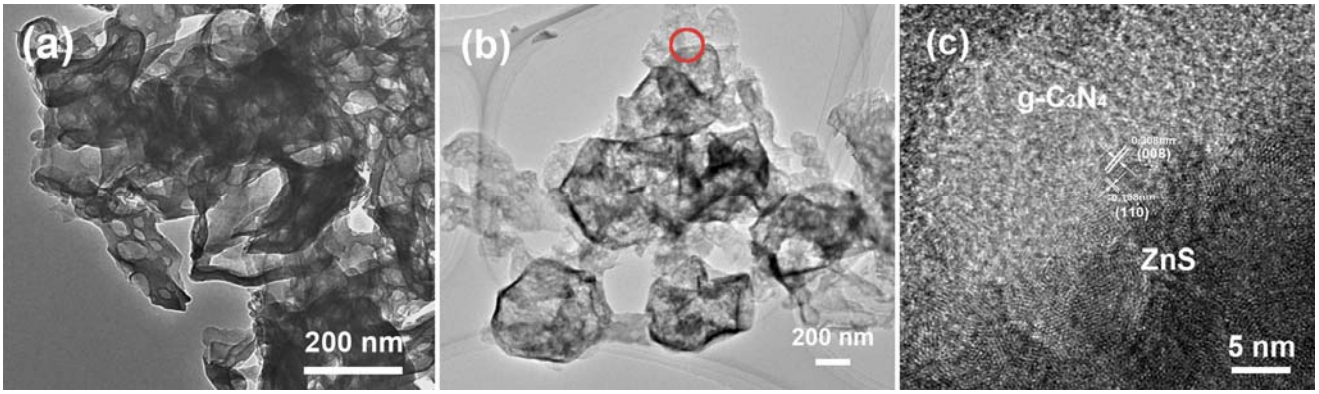

Figure 3. TEM images of (a) pure g-C_3N_4, (b) 6CNZS, and (c) HRTEM image of 6CNZS.

wurtzite ZnS. These results agree well with the XRD results in Figure 1. This tight coupling is favorable for the charge transfer between g-C_3N_4 and ZnS and it enhances the separation of electron-hole pairs and thus improves the photocatalytic activity. Moreover, the result indicates that the CNZS composites are heterogeneous in structure rather than being a mechanical mixture of the two separate components of g-C_3N_4 and ZnS.

Figure 4 shows the FT-IR spectra of ZnS, g-C_3N_4, as well as a series of CNZS photocatalysts with various ZnS content ratios. The top curve shows the spectrum of pure ZnS nanocages and the inset in Figure 4 depicts the detailed information of the wavenumbers between 1800 and 600 cm^{-1} for ZnS. The absorption band at 1622 cm^{-1} is ascribed to the N-H rocking mode in acetamide. Furthermore, those at 1570 and 1420 cm^{-1} are assigned to C=O stretching vibration in acetate, which is generated from the reactant for ZIF-8 templates. The band from the characteristic vibrations of ZnS at 647 cm^{-1} was observed, which further validated the formation of ZnS.[26] In the case of pure g-C_3N_4, the broad band between 3000 and 3500 cm^{-1} from the N-H stretching mode is presented as well as an overlapping band of OH stretching mode.[27, 28] The obvious absorption peak at 1626 cm^{-1} from the deformation mode of NH_2 is also found. In addition, the bands at 1200-1600 cm^{-1} are attributed to the typical stretching modes of aromatic CN heterocycles, which can be observed clearly in this figure.[24] Among them, the intense peaks at 1315 and 1226 cm^{-1} characterizes the C-N stretching vibration of connected units of C-N(-C)-C (full condensation) or C-NH-C (partial condensation).[28] Moreover, the sharp peak at about 806 cm^{-1} is related to the out-of-plane bending vibration characteristic of triazine or heptazine rings. As coupling ZnS with g-C_3N_4, the FT-IR spectra of CNZS composites are quite similar to those of the main peaks of pure g-C_3N_4, suggesting the maintenance of the g-C_3N_4 structure in the CNZS composites. However, it is worth noting that the peaks at 1315 and 1226 cm^{-1} for the pure g-C_3N_4 respectively shift to higher wavenumbers of 1322 and 1239 cm^{-1}, indicating the interactions between the Zn^{2+} and the N atoms in the CN heterocycle rings. This result further suggests that heterojunctions were successfully achieved in CNZS composite structures.

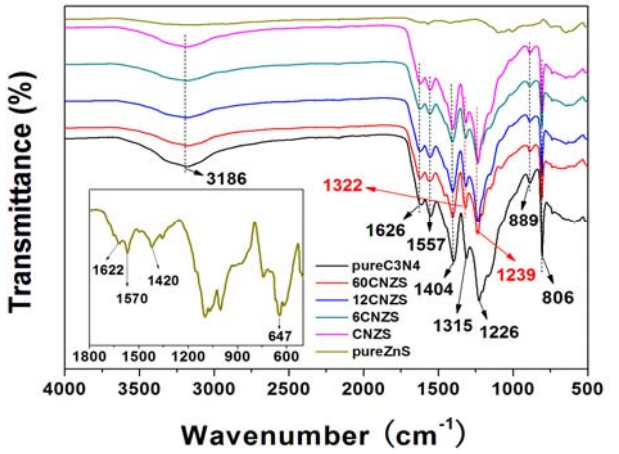

Figure 4. FT-IR spectra of pure g-C_3N_4, pure ZnS, and g-C_3N_4/ZnS composites.

The UV-vis diffuse reflectance spectra of ZnS, g-C_3N_4 and all CNZS composite photocatalysts are shown in Figure 5a. It is seen that the pure ZnS holds absorption edge of ~340 nm, which can be assigned to a band gap of around 3.6 eV.[29] The absorption edge of pristine g-C_3N_4 can be estimated at 460 nm, which corresponds to a band gap of 2.7 eV. This value is consistent with the previous reports.[7] Similarly to the pure g-C_3N_4, all the CNZS composites exhibit strong visible light absorption, which implies that they can successfully be used as visible light-driven photocatalysts.

The band gap energy of semiconductor can be calculated from the formula:

$$(\alpha h\nu)^n = k(h\nu - Eg) \quad (1)$$

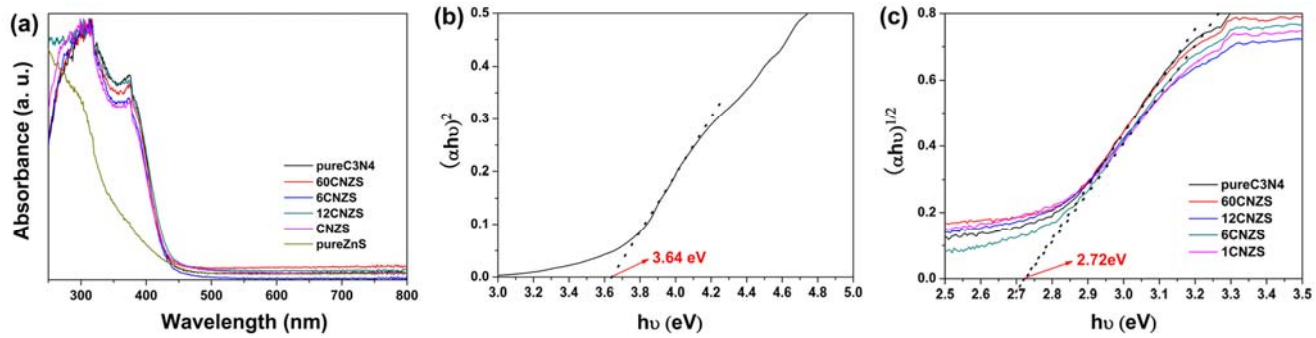

Figure 5. UV-vis diffuse reflectance spectra of pure g-C_3N_4, ZnS and CNZS samples (a), plot of $(\alpha hv)^2$ versus the photon energy of ZnS (b), and $(\alpha hv)^{1/2}$versus the photon energy of g-C_3N_4 and CNZS samples.

where hν is the photon energy, α is the absorption coefficient and k is a constant relative to the material. Moreover, n is a value that depends on the nature of the transition, which is either 2 for a direct transition or 1/2 for an indirect transition. For ZnS and pure g-C_3N_4, the values of n are 2 and 1/2, respectively. As shown in Figure 5b, the direct band gap of pure ZnS is estimated to be 3.64 eV, which indicates that pure ZnS cannot work as photocatalyst in the visible light region. Accordingly, as shown in Figure 5c, the band gap of g-C_3N_4 is determined from the plot of $(\alpha hv)^{1/2}$ *versus* energy (hv) and found to be 2.72 eV, consistent with the reported value previously.[7] After combining these two semiconductors, the band gaps of CNZS composite photocatalysts keep at around 2.72 eV, implying the composite photocatalysts is responsive in the visible-light region.

On the basis of the above results, we tested the photocatalytic performances of CNZS composites for the degradation of RhB under a visible light (λ> 400nm) irradiation. For the simplicity of analysis, the characteristic absorption peak at 553 nm was employed to determine the degradation degree of RhB. As shown in Figure 6a, no noticeable degradation of RhB was observed with pure ZnS nanocage photocatalyst. This is due to that ZnS with a wide band gap could not be excited by the visible light. Similar to previously reported results, pure g-C_3N_4 photocatalyst could degrade RhB by 75% in 90 min.[15] When coupling the two semiconductors, all of the CNZS composites exhibited a higher photocatalytic activity than either pure ZnS or pure g-C_3N_4 under visible light irradiation. Significantly, the photocatalytic activity of the composite photocatalyst was enhanced gradually with the increasing weight ratio of ZnS to g-C_3N_4 from 1:60 to 1:12. When the weight ratio reached 1:6, the as-prepared 6CNZS resulted in the highest activity. Specifically, it degraded more than 60% of RhB within 30 min and an almost complete decomposition was realized within 75 min. However, while further increasing the ZnS amount to the weight ratio of 1:1, the photocatalytic performance was decreased. Hence, the optimal weight ratio of g-C_3N_4 to ZnS is 6:1. For comparison, the widely-used photocatalyst of TiO_2 (P25) were also tested for the degradation of RhB under the same conditions. As expected, the visible inactive photocatalyst of P25 TiO_2 exhibited weak photocatalytic activity compared to the CNZS composite photocatalysts. Moreover, the temporal evolution of the spectral changes taking place during the photodegradation of RhB over the photocatalysts was shown in Figure S3.

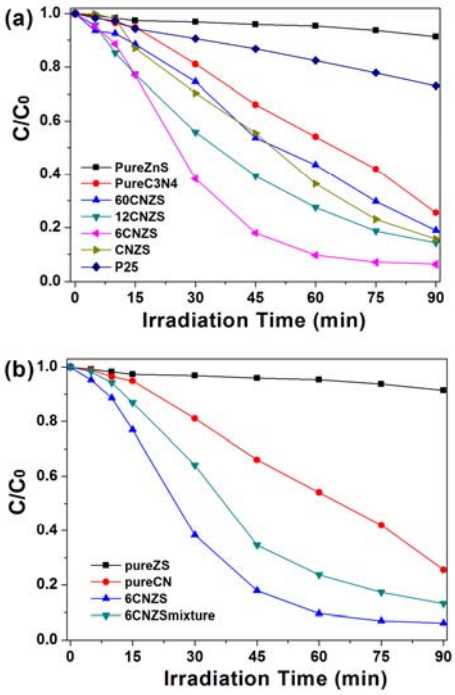

Figure 6. Visible light induced photocatalytic degradation of RhB by pure g-C3N4, ZnS nanocages, CNZS composites and P25 (a); comparison of photocatalytic activities of 6CNZS composites and mechanical mixture.

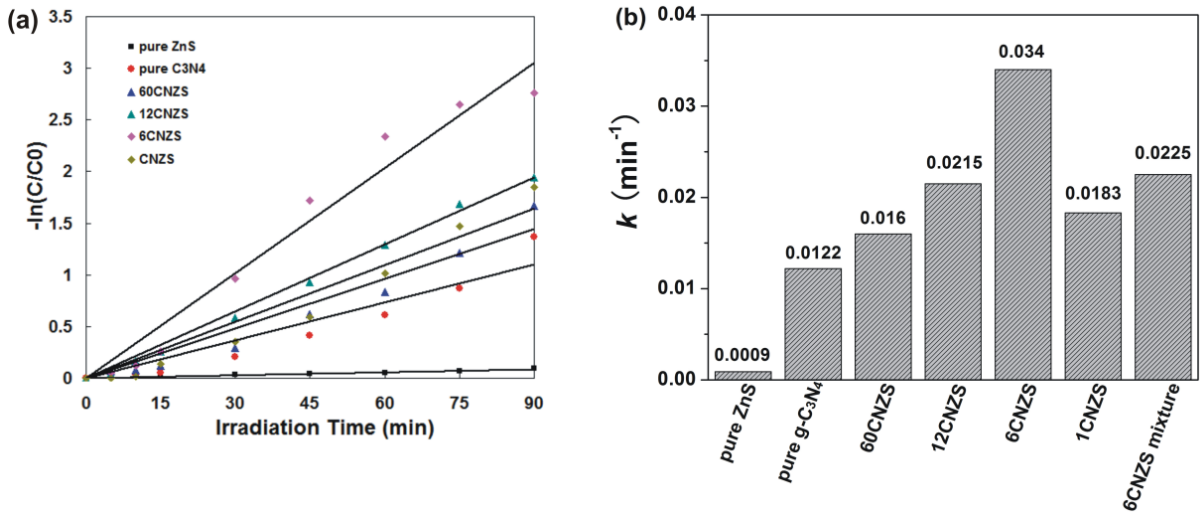

Figure 7. First-order kinetics plot for the photodegradation of RhB by g-C_3N_4, ZnS nanocages, and g-C_3N_4/ZnS heterojunctions (a) and their corresponding rate constants k (b).

To further investigate the heterojuction effect on the photocatalysts, the photocatalytic degradation of RhB over the mechanical mixture of 6CNZS sample was tested, as shown in Figure 6b. It is clear that the photocatalytic activity of a 6CNZS heterojuntion is higher than that of a mechanical mixture of a 6CNZS sample. This can be assigned to a more efficient separation of photo-excited electron-hole pairs benefiting from the intimately contacted interfaces in the 6CNZS heterojuntions. However, the relatively high photocatalytic activity shown in the mechanical mixture with weight ratio of 6:1 still shed some lights that the simple mixing might be good enough for quick test with other semiconductor composites.

To have a better understanding of the reaction kinetics of the RhB photodegradation catalyzed by different photocatalysts, the experimental data were fitted by a first-order model as expressed by the following equation:

$$-\ln(C/C_0) = kt \quad (2)$$

where k is the rate constant (min^{-1}), C_0 is the initial concentration of RhB, and C is the actual concentration of RhB at time t. The linear relationships between $-\ln(C/C_0)$ and the irradiation time are given in Figure 7a. Obviously, 6CNZS displays the best photocatalytic activity among all the tested composites photocatalysts with the highest rate constant of 0.034 min^{-1}. As shown in Figure 7b, the photocatalytic degradation rate of 6CNZS toward RhB is almost 37.8 and 2.8 times as high as those for individual ZnS and g-C_3N_4. In addition, the 6CNZS degradation rate is 2.1 and 1.6 times higher than that for 60CNZS and 12CNZS under the same experimental conditions, respectively. However, a further increase of the ZnS content to 1:1 led to a significant decrease of the RhB degradation rate. This can be attributed to the decreased weight ratio of the g-C_3N_4, which is the effective component that can be excited under visible light irradiation.

It is well known that photoluminescence (PL) analysis is commonly applied to investigate the photo-induced carrier separation efficiency of semiconductor photocatalyst.[22, 30] Figure 8 presents the PL spectra of pure g-C_3N_4 and 6CNZS composite with an excitation wavelength of 325 nm. As shown, the PL spectrum of pure g-C_3N_4 shows a strong PL emission band centered at 456 nm. This can be attributed to the band-band PL phenomenon with the energy of light approximately equal to the band gap of g-C_3N_4 (2.7 eV), which results from the n-π*transitions involving lone pairs of nitrogen atoms in the g-C_3N_4.[28] Obviously, a ZnS modification leads to a significant fluorescence quenching of the 6CNZS composite. In order to rule out the possibility that the PL intensity decreased when the g-C_3N_4 was diluted with ZnS in the composite, the intensity was normalized to the mass of g-C_3N_4. Therefore, the fluorescence quenching can be attributed to a decreased recombination of the electron-hole pairs in the composite system. Thus enhances light utilization and performs the better photocatalytic activity.

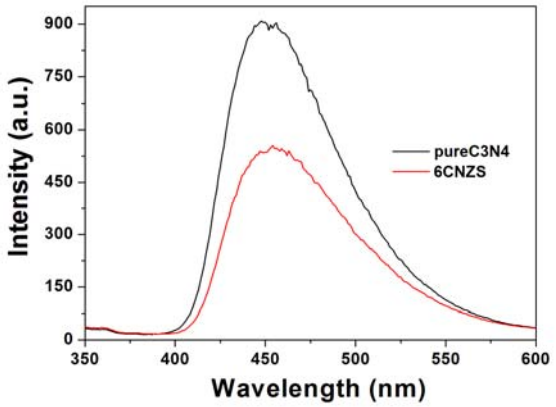

Figure 8. Photoluminescence (PL) spectra of g-C_3N_4 and 6CNZS composite.

In order to further reveal the photocatalytic mechanism of g-C_3N_4/ZnS composites, the reactive species trapping experiments were conducted to probe the main active species in the photocatalytic process. In this study, *tert*-butyl alcohol (TBA), disodium ethylenediaminetetraacetate (Na_2-EDTA) and p-benzoquinone (BQ) were employed as scavengers for hydroxyl radicals (OH·), photogenerated holes (h^+) and superoxide radicals ($\cdot O_2^-$), respectively. As shown in Figure 9, when the scavenger for hydroxyl radical (TBA, 50μL) was added, the photocatalytic degradation of RhB was improved slightly compared to the performance of 6CNZS. This result indicated that OH· was not the active specie for the photocatalysis. Further, the photocatalytic activity was enhanced significantly with the addition of hole-scavenger, suggesting that h^+ was also not the main active specie for the photocatalytic degradation. This enhancement of photocatalytic activity can be attributed to an efficient separation for photo-induced electron-hole pairs, which results from the trapping of holes by scavengers (Na_2-EDTA, 2mM). On the contrary, the introduction of scavenger for $\cdot O_2^-$ (BQ, 0.5mM) resulted in a remarkable deactivation of the 6CNZS composite photocatalyst. This result clearly implies that superoxide radicals $\cdot O_2^-$ are the main contributions to the photocatalytic performance.

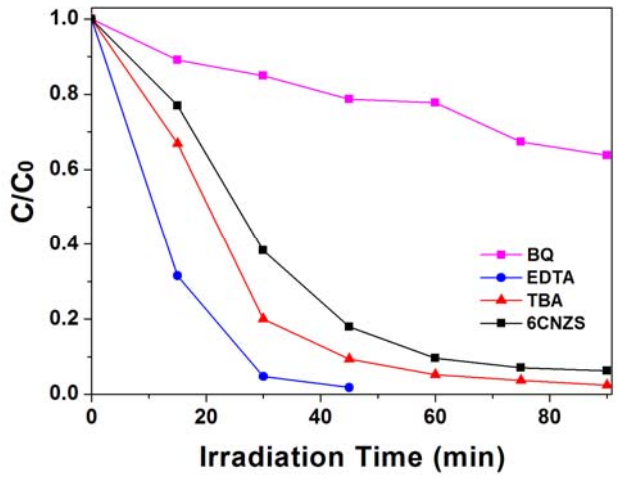

Figure 9. Photocatalytic degradation of RhB over 6CNZS composite with and without the addition of BQ, EDTA and TBA.

On the basis of experimental results and theoretical analysis, a possible synergistic mechanism between g-C_3N_4 and ZnS for a photodegradation of RhB was proposed as illustrated in Figure 10. Under the visible light irradiation, g-C_3N_4 can be excited due to the appropriate band gap (2.7 eV). However, ZnS is inert owing to its wide band gap. Subsequently, the photo-excited electrons on g-C_3N_4 could be directly injected into the CB of ZnS through the well-developed interfaces. This is due to that the conduction band of g-C_3N_4 (-1.13 eV) is more negative than that of ZnS (-1.05 eV). The charge transfer effectively inhibits the recombination of photogenerated electrons-holes pairs and thus enhances the photocatalytic activity. The photoinduced electrons diffused to the surface and reacted with oxygen molecule which is well-known as electron acceptor, generating superoxide radicals $\cdot O_2^-$. The active superoxide radicals are of high oxidation activity, which can decompose RhB finally.

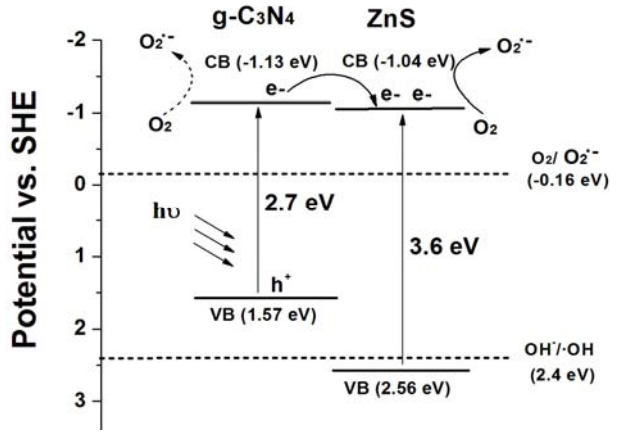

Figure 10. Proposed mechanism for the photodegradation of RhB on CNZS composites.

4. Conclusions

In summary, g-C_3N_4/ nanocage ZnS composites were fabricated using ZIF-8 as self-sacrificing template. The resulting CNZS heterojunctions were found to enhance photocatalytic activity under visible light irradiation for a degradation of RhB. This can be attributed to the well-aligned band structures of g-C_3N_4 and ZnS. Moreover, the thin shell and flat surface of the ZnS nanocage provides an intimate contacting interface with g-C_3N_4, through which the photogenerated electron-hole pairs can transfer and separate efficiently and thus prohibit the recombination of elctron-hole pairs. The optimum photocatalytic activity of 6CNZS for RhB degradation was almost 37.8 and 2.8 times higher than those of the individual ZnS and g-C_3N_4, respectively. The results indicated that the 6CNZS composite prepared in this work exhibits a great potential to be applied in environmental issues. Here, an efficient synthesis method for CNZS heterojunctions is of significant interest for pollutants degradation and could be a new method to design new photocatalysts with high performance of environmental applications.

Acknowledgements

Jing Wang is very grateful for the financial support of Chinese Scholarship Council for her stay in Sweden.

Notes and references

[a] Department of Materials Science and Engineering, KTH Royal Institute of Technology, Stockholm, SE-10044, Sweden.
[b] Department of Materials and Environmental Chemistry, Stockholm University, Stockholm, SE-10691, Sweden

[c] Department of Materials Science and Engineering, Shanghai Institute of Technology, Shanghai, 201418, P.R. China.
Corresponding Author:
* zhezhao@kth.se, jiwa@kth.se. Phone: (+46)-87908324
Electronic Supplementary Information (ESI) available: [The HRTEM image of ZnS nanocages, XRD patterns of the CNZS composite photocatalysts and the temporal evolution of the spectral changes taking place during the photodegradation of RhB over the photocatalysts]. See DOI: 10.1039/b000000x/

1. X. Han, Q. Kuang, M. Jin, Z. Xie and L. Zheng, *Journal of the American Chemical Society*, 2009, **131**, 3152-3153.
2. X. Hu, G. Li and J. C. Yu, *Langmuir*, 2009, **26**, 3031-3039.
3. J. Zhuang, W. Dai, Q. Tian, Z. Li, L. Xie, J. Wang, P. Liu, X. Shi and D. Wang, *Langmuir*, 2010, **26**, 9686-9694.
4. Z. Liu, D. D. Sun, P. Guo and J. O. Leckie, *Chem-Eur J*, 2007, **13**, 1851-1855.
5. Y. Zheng, Y. Jiao, J. Chen, J. Liu, J. Liang, A. Du, W. Zhang, Z. Zhu, S. C. Smith, M. Jaroniec, G. Q. Lu and S. Z. Qiao, *Journal of the American Chemical Society*, 2011, **133**, 20116-20119.
6. F. Goettmann, A. Fischer, M. Antonietti and A. Thomas, *New J Chem*, 2007, **31**, 1455-1460.
7. X. Wang, K. Maeda, A. Thomas, K. Takanabe, G. Xin, J. M. Carlsson, K. Domen and M. Antonietti, *Nat Mater*, 2009, **8**, 76-80.
8. L. Huang, H. Xu, Y. Li, H. Li, X. Cheng, J. Xia, Y. Xu and G. Cai, *Dalton Transactions*, 2013, **42**, 8606-8616.
9. S. C. Yan, Z. S. Li and Z. G. Zou, *Langmuir*, 2009, **25**, 10397-10401.
10. J.-X. Sun, Y.-P. Yuan, L.-G. Qiu, X. Jiang, A.-J. Xie, Y.-H. Shen and J.-F. Zhu, *Dalton Transactions*, 2012, **41**, 6756-6763.
11. J. Fu, Y. Tian, B. Chang, F. Xi and X. Dong, *Journal of Materials Chemistry*, 2012, **22**, 21159-21166.
12. Y. Tian, B. Chang, J. Lu, J. Fu, F. Xi and X. Dong, *ACS applied materials & interfaces*, 2013, **5**, 7079-7085.
13. J. Zhang, Y. Wang, J. Jin, J. Zhang, Z. Lin, F. Huang and J. Yu, *ACS Applied Materials & Interfaces*, 2013, **5**, 10317-10324.
14. J. Fu, B. Chang, Y. Tian, F. Xi and X. Dong, *Journal of Materials Chemistry A*, 2013, **1**, 3083-3090.
15. Y. He, J. Cai, T. Li, Y. Wu, Y. Yi, M. Luo and L. Zhao, *Ind Eng Chem Res*, 2012, **51**, 14729-14737.
16. K.-i. Katsumata, R. Motoyoshi, N. Matsushita and K. Okada, *Journal of Hazardous Materials*, 2013, **260**, 475-482.
17. S. C. Yan, S. B. Lv, Z. S. Li and Z. G. Zou, *Dalton Transactions*, 2010, **39**, 1488-1491.
18. X. Xu, G. Liu, C. Randorn and J. T. S. Irvine, *International Journal of Hydrogen Energy*, 2011, **36**, 13501-13507.
19. B. Chai, X. Liao, F. Song and H. Zhou, *Dalton Transactions*, 2013.
20. M. Xu, L. Han and S. Dong, *ACS Applied Materials & Interfaces*, 2013, **5**, 12533-12540.
21. J. Hong, Y. Wang, Y. Wang, W. Zhang and R. Xu, *ChemSusChem*, 2013, **6**, 2263-2268.
22. Y. Li, H. Zhang, P. Liu, D. Wang, Y. Li and H. Zhao, *Small*, 2013, **9**, 3336-3344.
23. Z. Jiang, H. Sun, Z. Qin, X. Jiao and D. Chen, *Chemical Communications*, 2012, **48**, 3620-3622.
24. F. Dong, L. Wu, Y. Sun, M. Fu, Z. Wu and S. Lee, *Journal of Materials Chemistry*, 2011, **21**, 15171-15174.
25. Y. Zhang, J. Liu, G. Wu and W. Chen, *Nanoscale*, 2012, **4**, 5300-5303.
26. S. Chen and W. Liu, *Langmuir*, 1999, **15**, 8100-8104.
27. S. Yang, Y. Gong, J. Zhang, L. Zhan, L. Ma, Z. Fang, R. Vajtai, X. Wang and P. M. Ajayan, *Advanced Materials*, 2013, **25**, 2452-2456.
28. V. N. Khabashesku, J. L. Zimmerman and J. L. Margrave, *Chem Mater*, 2000, **12**, 3264-3270.
29. Y. Xu and M. A. A. Schoonen, *Am Mineral*, 2000, **85**, 543-556.
30. L. K. van Vugt, S. J. Veen, E. P. A. M. Bakkers, A. L. Roest and D. Vanmaekelbergh, *Journal of the American Chemical Society*, 2005, **127**, 12357-12362.

